Article

Not peer-reviewed version

Stochastic strike-slip fault as earthquake source model

Maksim Gapeev , Alexandra Solodchuk , Roman Parovik *

Posted Date: 11 August 2023

doi: 10.20944/preprints202308.0919.v1

Keywords: stochastic fault surface; earthquake source model; elasticity theory

Article

Stochastic Strike-Slip Fault as Earthquake Source Model

Maksim Gapeev, Alexandra Solodchuk and Roman Parovik *

Institute of Cosmophysical Research and Radio Wave Propagation FEB RAS, 7 Mirnaya Str., Paratunka, Kamchatka, 684034, Russia

* Correspondence: romanparovik@gmail.com (R.P.)

Abstract: It is known that the source of a tectonic earthquake in the framework of the theory of elasticity and viscoelasticity is considered as a displacement along a certain fault surface. Usually, when describing the source, the geometry of the fault surface is simplified to a flat rectangular area. The displacement vector is assumed to be constant. In this paper, we propose a model of an earthquake source in the form of a displacement with a constant vector along a stochastic surface. A number of standard assumptions were made when modeling. We take into account only the elastic properties of the medium. We consider the Earth's crust as a half-space and assume that the medium is homogeneous and isotropic. For the mathematical description of the earthquake source, we use the classical force equivalent of displacement along the fault. This is the distribution of double pairs of forces. The field of displacements under the action of body forces is found through a combination of Mindlin nuclei of strain. The paper presents solutions for strike-slip fault. To obtain a stochastic fault surface, we propose to introduce a random deformation of a rectangular flat surface. The paper presents the results of a computational experiment comparing the levels and regions of relative deformations of the Earth's crust in the case of displacement along a flat rupture surface and along a stochastic one. In the case of a stochastic surface, the regions of relative deformations become asymmetric. The developed model will help to indirectly take into account various mechanical properties of the Earth's crust when modeling deformations caused by earthquakes.

Keywords: stochastic fault surface; earthquake source model; elasticity theory

MSC: 74B05; 86A17

1. Introduction

The source of a tectonic earthquake occurs as a result of the complete or partial relaxation of stress accumulated by the Earth's material during tectonic deformation. At this time, there is a local loss of stability of the medium, its continuity is violated [1]. As a result, the accumulated elastic strain energy transforms into inelastic one. In the framework of the theory of elasticity and viscoelasticity, the earthquake source is considered as a dislocation, i.e. displacement along a certain fault surface [2]. In addition to the geometry of this surface, the earthquake source is characterized by orientation and position in space, as well as by the field of the slip vector along the rupture surface. When describing the source, the following assumptions are most often used: the surface geometry is simplified to a flat rectangular area [3–5], and the displacement vector is assumed to be constant [6,7]. Such simplifications make it possible to obtain analytical solutions to the problem of determining the displacement field of the Earth's crust at the time of an earthquake [8].

The Earth's crust consists of separate layers of rocks. They have various mechanical properties. Direct consideration of these properties when constructing models of mechanical processes occurring in rocks is difficult. It is possible to indirectly take into account the mechanical properties of rocks by introducing stochastic components. Thus, the problem of the probabilistic characteristics of the displacement vector in the earthquake source was previously investigated [9]. It was shown that the probability distribution of the normalized displacement value has a stability. It is similar to the

Preprints (www.preprints.org) | NOT PEER-REVIEWED | Posted: 11 August 2023 doi:10.20944/preprints202308.0919.v1

exponential one, but has a heavy tail. In addition, a compact description of the distribution was proposed using the lognormal law with a negative shift of the density function and winsorization at zero. The described approach, as well as similar ones, were used in modeling displacements of the Earth's surface to calculate the strength of engineering structures [10–12]. Also the effect of adding a slip deficit to the stochastic fault model on the slip distribution in the subduction zone was considered [13]. An overview of the methods for adding stochastic components into the earthquake source model is presented in Gusev's paper [14].

The geometric shape of the fault surface is one of the main characteristics of the earthquake source. Usually, when modeling a source, the fault surface is considered as a plane bounded by a rectangular region or as a composition of such regions [15–17]. In this paper, we propose a modified dislocation model of an earthquake source in the form of displacement along a stochastic surface.

The structure of the main part of the paper is as follows. Section 2 is devoted to the mathematical formulation of the problem of the stress-strain state of the Earth's crust in the elastic half-space approximation based on the Navier equations. Earthquake source modeling based on systems of equivalent forces is carried out. Solutions are derived for determining the deformations of an elastic half-space under the action of a dislocation along an arbitrary smooth surface. A method for constructing a stochastic displacement surface in an earthquake source is described. Section 3 contains the results of numerical modeling of the Earth's crust deformations. The main findings and conclusion are contained in Section 4.

2. Mathematical formulation

2.1. Stress-strain state of the Earth's crust

We make a number of standard assumptions when modeling [18]. We will take into account only the elastic properties of the medium, we will simplify the geometry of the Earth's crust to a half-space, and we will assume that the medium is homogeneous and isotropic. To describe such a model in a Cartesian coordinate system (x_1, x_2, x_3) let's use the Navier equations [19] :

$$\mu \frac{\partial^2 u_i}{\partial x_j^2} + (\lambda + \mu) \frac{\partial^2 u_i}{\partial x_i \partial x_j} + X_i = 0, \; i, j = 1..3, \tag{1}$$

where u_i are displacement vector components, X_i are body forces, λ, μ are Lame coefficients.

The boundary conditions of the problem (1) are defined on the surface $x_3 = 0$ and consist in the equality of the following components of the stress tensor to zero:

$$\sigma_{31}|_{x_3=0} = \sigma_{32}|_{x_3=0} = \sigma_{33}|_{x_3=0} = 0. \tag{2}$$

According to modern concepts, tectonic earthquake source occurs as a result of sliding along the inner surface – the fault plane [1]. Mathematically, earthquake sources are described by a body force within the excitation area, a displacement jump on the fault surface, or deformation. Note that the displacement along the fault excites the same seismic waves as some system of forces distributed over the fault with zero total moment. In general, the distribution of forces can have a different form, but in the case of an isotropic medium, it can always be chosen as the surface distribution of double pairs of forces. The classical force equivalent of displacement along a fault is the distribution of double pairs of forces.

2.2. Point source. Mindlin solutions

Mindlin [20,21] was engaged in solving the problem of determining the displacement field under the action of body forces located inside an elastic half-space and applied to one point. In his works, he solved this problem for differently directed single and double forces, including double forces with moments. Mindlin expressed his solutions in terms of combinations of strain nuclei for elastic space

Preprints (www.preprints.org) | NOT PEER-REVIEWED | Posted: 11 August 2023 doi:10.20944/preprints202308.0919.v1

proposed by Kelvin. Mindlin solutions can also be called strain nuclei for an elastic half-space by analogy with the Kelvin solutions. Solutions of the differential equations system (1) with boundary conditions (2) can be expressed through these nuclei. Mindlin expressed the solutions in terms of the Galerkin vector. In the present work, equivalent solutions are constructed in the form of displacement vector components.

We take a Cartesian coordinate system. Let u_i^j be the i-th component of the displacement vector at the point (x_1, x_2, x_3), corresponding to the single force of magnitude F at the point (ξ_1, ξ_2, ξ_3) in the direction j. According to Mindlin's works u_i^j can be represented as follows:

$$\begin{aligned} u_i^j(x_1,x_2,x_3) =& u_{iA}^j(x_1,x_2,-x_3) - u_{iA}^j(x_1,x_2,x_3) + \\ &+ u_{iB}^j(x_1,x_2,x_3) + x_3 u_{iC}^j(x_1,x_2,x_3) \end{aligned} \tag{3}$$

$$\begin{cases} u_{iA}^j = \dfrac{F}{8\pi\mu}\left[(2-\alpha)\dfrac{\delta_{ij}}{R} + \alpha\dfrac{R_iR_j}{R^3}\right] \\ u_{iB}^j = \dfrac{F}{4\pi\mu}\left[\dfrac{\delta_{ij}}{R} + \dfrac{R_iR_j}{R^3} + \dfrac{1-\alpha}{\alpha}\left(\dfrac{\delta_{ij}}{R+R_3} + \dfrac{R_i\delta_{j3} - R_j\delta_{i3}(1-\delta_{j3})}{R(R+R_3)} - \right.\right. \\ \quad \left.\left. - \dfrac{R_iR_j}{R(R+R_3)^2}(1-\delta_{i3})(1-\delta_{j3})\right)\right] \\ u_{iC} = \dfrac{F}{4\pi\mu}(1-2\delta_{i3})\left[(2-\alpha)\dfrac{R_i\delta_{j3} - R_j\delta_{i3}}{R^3} + \alpha\xi_3\left(\dfrac{\delta_{ij}}{R^3} - \dfrac{3R_iR_j}{R^5}\right)\right], \end{cases} \tag{4}$$

where $\alpha = (\lambda+\mu)/(\lambda+2\mu)$, δ_{ij} is Kronecker delta, $R_1 = x_1 - \xi_1$, $R_2 = x_2 - \xi_2$, $R_3 = -x_3 - \xi_3$, $R^2 = R_1^2 + R_2^2 + R_3^2$.

To obtain solutions in the form of strain nuclei, we will take the corresponding partial ξ_k derivatives of $u_i^j(x_1, x_2, x_3)$:

$$\begin{aligned} \frac{\partial u_i^j(x_1,x_2,x_3)}{\partial\xi_k} =& \frac{\partial u_{iA}^j(x_1,x_2,-x_3)}{\partial\xi_k} - \frac{\partial u_{iA}^j(x_1,x_2,x_3)}{\partial\xi_k} + \\ &+ \frac{u_{iB}^j(x_1,x_2,x_3)}{\partial\xi_k} + x_3\frac{\partial u_{iC}^j(x_1,x_2,x_3)}{\partial\xi_k} \end{aligned} \tag{5}$$

$$\begin{cases} \dfrac{\partial u_{iA}^j}{\partial\xi_k} = \dfrac{F}{8\pi\mu}\left\{(2-\alpha)\dfrac{R_k}{R^3}\delta_{ij} - \alpha\dfrac{R_i\delta_{jk} + R_j\delta_{ik}}{R^3} + 3\alpha\dfrac{R_iR_jR_k}{R^5}\right\} \\ \dfrac{\partial u_{iB}^j}{\partial\xi_k} = \dfrac{F}{4\pi\mu}\left\{-\dfrac{R_i\delta_{jk} + R_j\delta_{ik} - R_k\delta_{ij}}{R^3} + \dfrac{3R_iR_jR_k}{R^5} + \right. \\ \quad + \dfrac{1-\alpha}{\alpha}\left[\dfrac{\delta_{3k}R + R_k}{R(R+R_3)^2}\delta_{ij} - \dfrac{\delta_{ik}\delta_{j3} - \delta_{jk}\delta_{i3}(1-\delta_{j3})}{R(R+R_3)} + \right. \\ \quad + [R_i\delta_{j3} - R_j\delta_{i3}(1-\delta_{j3})]\dfrac{\delta_{3k}R^2 + R_k(2R+R_3)}{R^3(R+R_3)^2} + \left[\dfrac{R_i\delta_{jk} + R_j\delta_{ik}}{R(R+R_3)^2} - \right. \\ \quad \left.\left.\left. - R_iR_j\dfrac{2\delta_{3k}R^2 + R_k(3R+R_3)}{R^3(R+R_3)^3}\right](1-\delta_{i3})(1-\delta_{j3})\right]\right\} \\ \dfrac{\partial u_{iC}^j}{\partial\xi_k} = \dfrac{F}{4\pi\mu}(1-2\delta_{i3})\left\{(2-\alpha)\left[\dfrac{\delta_{jk}\delta_{i3} - \delta_{ik}\delta_{j3}}{R^3} + \right.\right. \\ \quad \left.\left. + \dfrac{3R_k(R_i\delta_{j3} - R_j\delta_{i3})}{R^5}\right] + \alpha\left[\dfrac{\delta_{ij}}{R^3} - \dfrac{3R_iR_j}{R^5}\right]\delta_{3k} + \right. \\ \left. + 3\alpha\xi_3\left[\dfrac{R_i\delta_{jk} + R_j\delta_{ik} + R_k\delta_{ij}}{R^5} - \dfrac{5R_iR_jR_k}{R^7}\right]\right\} \end{cases} \tag{6}$$

Preprints (www.preprints.org) | NOT PEER-REVIEWED | Posted: 11 August 2023 doi:10.20944/preprints202308.0919.v1

2.3. Distributed source

Using the Volterra dislocation principle, Steketee showed [2] that the displacement field caused by movement along the fault plane Σ in an elastic half-space can be found through a surface integral of the following form:

$$u_i = \frac{1}{F} \iint\limits_{\Sigma} \Delta u_j \left[\lambda \delta_{kj} \frac{\partial u_i^n}{\partial \xi_n} + \mu \left(\frac{\partial u_i^k}{\partial \xi_j} + \frac{\partial u_i^j}{\partial \xi_k} \right) \right] \nu_j \, d\Sigma, \tag{7}$$

where Δu_j is a dislocation in the j – th direction across the fault surface Σ, ν_j are the direction cosines of the normal to the surface element $d\Sigma$, u_i^j is the i-th component of the displacement vector at the point (x_1, x_2, x_3), corresponding to the single force in j direction with magnitude F at the point (ξ_1, ξ_2, ξ_3). If $k = j$, then $\partial u_i^k / \partial \xi_j$ are strain nuclei corresponding to a double forces without moment (Figure 1a), and $\partial u_i^n / \partial \xi_n$ is the strain nuclei combination corresponding to the dilation center. If $k \neq j$, then $(\partial u_i^k / \partial \xi_j + \partial u_i^j / \partial \xi_k)$ are strain nuclei corresponding to two perpendicular pairs of double forces with moments (Figure 1b). Figure 1 shows the systems of forces corresponding to strain nuclei combinations $\partial \mathbf{u}^k / \partial \xi_j + \partial \mathbf{u}^j / \partial \xi_k$.

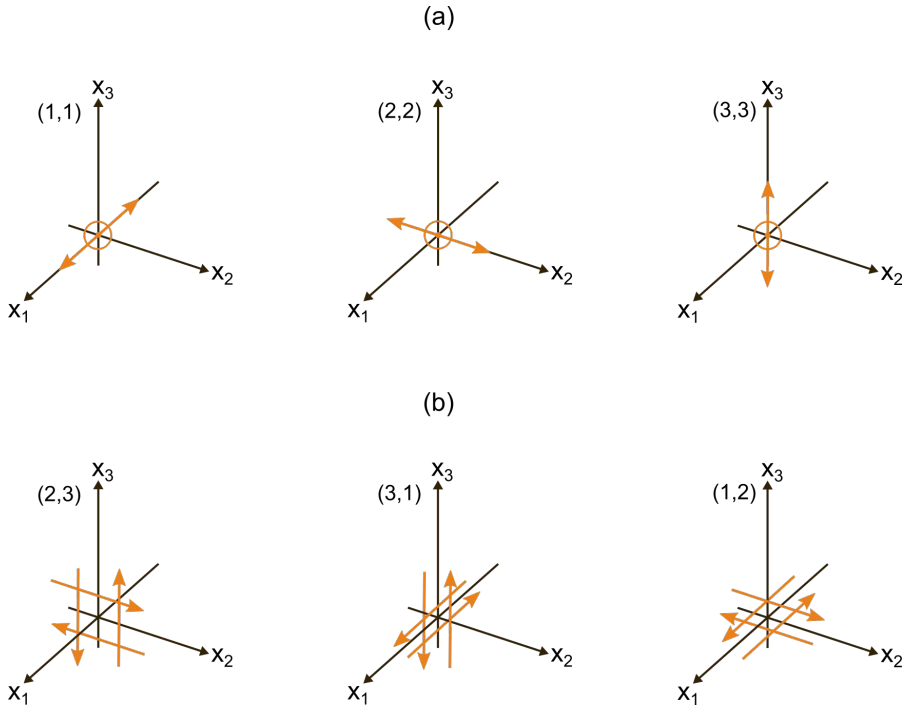

Figure 1. Systems of forces required to obtain the force equivalent of displacement: pairs of forces without moments **(a)** and mutually perpendicular pairs of double forces with moments relative to the coordinate axes **(b)**. The numbers in brackets correspond to the indices (k, j) from equation (7).

In this paper, we will consider earthquake source of strike-slip type . The strain nuclei combination for such an earthquake source is as follows:

$$\begin{aligned} u_i = \frac{1}{F} \iint\limits_{\Sigma} \Delta u_1 \Big\{ \Big[\lambda \Big(\frac{\partial u_i^2}{\partial \xi_2} + \frac{\partial u_i^3}{\partial \xi_3} \Big) + (\lambda + 2\mu) \frac{\partial u_1^n}{\partial \xi_1} \Big] \nu_1 + \\ + \Big[\mu \Big(\frac{\partial u_i^1}{\partial \xi_2} + \frac{\partial u_i^2}{\partial \xi_1} \Big) \Big] \nu_2 + \Big[\mu \Big(\frac{\partial u_i^1}{\partial \xi_3} + \frac{\partial u_i^3}{\partial \xi_1} \Big) \Big] \nu_3 \Big\} d\Sigma. \end{aligned} \tag{8}$$

Let the fault surface Σ be explicitly given by the equation $\xi_2 = f(\xi_1, \xi_3)$. In this case, the unit normal $\boldsymbol{\nu}$ at each point $\xi(\xi_1, \xi_2, \xi_3)$ of the surface can be found as follows:

Preprints (www.preprints.org) | NOT PEER-REVIEWED | Posted: 11 August 2023 doi:10.20944/preprints202308.0919.v1

$$\boldsymbol{\nu}(\xi_1,\xi_2,\xi_3) = \frac{\left(\frac{df}{d\xi_1}, -1, \frac{df}{d\xi_3}\right)}{\sqrt{\left(\frac{df}{d\xi_1}\right)^2 + 1 + \left(\frac{df}{d\xi_3}\right)^2}}. \tag{9}$$

We denote the integrand (8) by $\Omega_{strike}(\xi_1,\xi_2,\xi_3)$:

$$\begin{aligned}\Omega^i_{strike}(\xi_1,\xi_2,\xi_3) = \Delta u_1 \Big\{ \Big[\lambda\Big(\frac{\partial u^2_i}{\partial \xi_2} + \frac{\partial u^3_i}{\partial \xi_3}\Big) + (\lambda+2\mu)\frac{\partial u^n_1}{\partial \xi_1}\Big]\nu_1 + \\ + \Big[\mu\Big(\frac{\partial u^1_i}{\partial \xi_2} + \frac{\partial u^2_i}{\partial \xi_1}\Big)\Big]\nu_2 + \Big[\mu\Big(\frac{\partial u^1_i}{\partial \xi_3} + \frac{\partial u^3_i}{\partial \xi_1}\Big)\Big]\nu_3 \Big\}\end{aligned} \tag{10}$$

We place the fault surface Σ at the depth $C < 0$. The projection $D_{x_1x_3}$ of this surface onto the plane $x_2 = 0$ is a rectangular area.

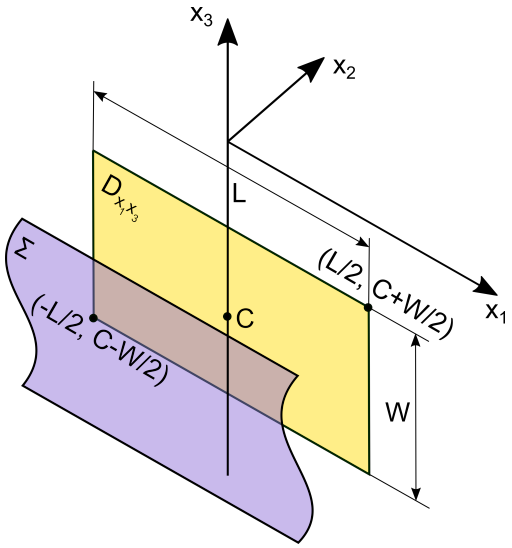

Figure 2. The fault surface Σ and its projection $D_{x_1x_3}$ onto the plane $x_2 = 0$.

Let us perform parametrization and move from surface integral to double, and then to iterated one:

$$u_i = \frac{1}{F}\int\limits_{-L/2}^{L/2} d\xi_1 \int\limits_{C-W/2}^{C+W/2} \Omega^i_{slip}(\xi_1, f(\xi_1,\xi_3),\xi_3)\sqrt{\left(\frac{df}{d\xi_1}\right)^2 + 1 + \left(\frac{df}{d\xi_3}\right)^2}\, d\xi_3. \tag{11}$$

This expression (11) allows us to calculate the components of the displacement field vector. The field arises as a result of displacement along the fault surface inside the elastic half-space in the strike direction.

2.4. Dislocation with a constant displacement vector along a finite rectangular surface

We represent the displacement surface Σ as a plane bounded by a rectangular region with dip angle δ. In this case, the unit normal is $\boldsymbol{\nu} = (0, -\sin(\delta), \cos(\delta))$. The displacement vector $\Delta\mathbf{u}$ is assumed to be constant. Its components in the case of displacement along strike are equal to $\Delta u_j = (U, 0, 0)$, and in the case of displacement along dip: $\Delta u_j = (0, U\cos(\delta), U\sin(\delta))$.

In this case, the integral (8) will take the form:

Preprints (www.preprints.org) | NOT PEER-REVIEWED | Posted: 11 August 2023 doi:10.20944/preprints202308.0919.v1

$$u_i = \frac{\mu U}{F} \iint\limits_{\Sigma} \Big[-\Big(\frac{\partial u_i^1}{\partial \xi_2} + \frac{\partial u_i^2}{\partial \xi_1} \Big) \sin(\delta) + \Big(\frac{\partial u_i^1}{\partial \xi_3} + \frac{\partial u_i^3}{\partial \xi_1} \Big) \cos(\delta) \Big] d\Sigma. \tag{12}$$

Given that the surface Σ is defined by the relation: $\xi_2 = (\xi_3 - C) \cdot \mathrm{ctg}(\delta)$, the surface integral will look like this:

$$u_i = \frac{1}{\sin(\delta) F} \int\limits_{-L/2}^{L/2} d\xi_1 \int\limits_{C - \frac{W \sin(\delta)}{2}}^{C + \frac{W \sin(\delta)}{2}} \Omega_{slip}^i(\xi_1, (\xi_3 - C) \cdot \mathrm{ctg}(\delta), \xi_3) d\xi_3. \tag{13}$$

2.5. Stochastic geometry of the fault surface

To obtain a stochastic fault surface Σ, we propose to introduce a random deformation of a rectangular flat surface Θ. For this:

1. We build a two-dimensional grid on the plane Θ with horizontal and vertical steps h_1 and h_2 respectively (Figure 3a).
2. We define a random function $\eta = \eta(\xi_1, \xi_3)$. For simplicity, we assume that $\eta(\xi_1, \xi_3)$ is characterized by a single distribution function for all values of the arguments ξ_1, ξ_3. The function $\eta(\xi_1, \xi_3)$ at each grid node (a_i, c_j) determines the value $b_{ij} = \eta(a_i, c_j)$. These values are the stochastic deformation component of the original plane Θ (Figure 3b).
3. The resulting fault surface Σ will be determined by the two-dimensional Lagrange interpolation polynomial $P(\xi_1, \xi_3)$ constructed from the points (a_i, b_{ij}, c_j) as follows:

$$P(\xi_1, \xi_3) = \sum_{j=1}^{n} \sum_{k=1}^{m} b_{ik} \frac{W_j(\xi_1)}{W_j(a_i)} \frac{V_k(\xi_3)}{V_k(c_k)}, \tag{14}$$

where $W_j(\xi_1)$ and $V_k(\xi_3)$ are functions defined in terms of polynomials $W(\xi_1) = (\xi_1 - a_1)(\xi_2 - a_2) \cdot \ldots \cdot (\xi_1 - a_n)$ and $V(\xi_3) = (\xi_3 - c_1)(\xi_2 - c_2) \cdot \ldots \cdot (\xi_1 - c_n)$:

$$W_j(\xi_1) = \frac{W(\xi_1)}{\xi_1 - a_j} = (\xi_1 - a_i) \cdot \ldots \cdot (\xi_1 - a_{j-1}) \cdot (\xi_1 - a_{j+1}) \cdot \ldots \cdot (\xi_1 - a_n), \tag{15}$$

$$V_k(\xi_3) = \frac{V(\xi_3)}{\xi_3 - c_k} = (\xi_3 - c_i) \cdot \ldots \cdot (\xi_3 - c_{j-1}) \cdot (\xi_3 - c_{j+1}) \cdot \ldots \cdot (\xi_3 - c_m). \tag{16}$$

Preprints (www.preprints.org) | NOT PEER-REVIEWED | Posted: 11 August 2023 doi:10.20944/preprints202308.0919.v1

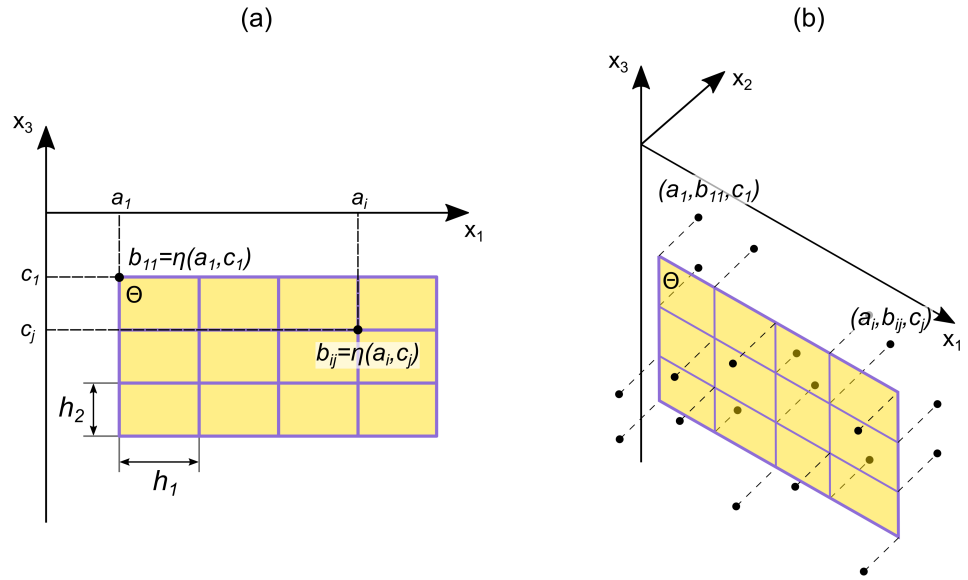

Figure 3. Scheme of stochastic deformation of a flat surface bounded by a rectangular area. Explanations are in the text above.

Solutions for displacement on such a surface Σ in the strike direction can be obtained using the integral (11), setting the function $f(\xi_1, \xi_3) = P(\xi_1, \xi_3)$. The internal strain and stress fields can be evaluated using the following relations:

$$e_{ij} = \frac{1}{2}\left(\frac{\partial u_i}{\partial x_j} + \frac{\partial u_j}{\partial x_i}\right), \tag{17}$$

$$\sigma_{ij} = \lambda e_{kk}\delta_{ij} + 2\mu e_{ij}. \tag{18}$$

Shear stresses [22–24] make the greatest contribution to the destruction of rocks. Therefore, to assess the deformations of the Earth's crust, we use the criterion of maximum shear stresses:

$$\tau_{\max} = \frac{1}{2}\max(|\sigma_1 - \sigma_2|, |\sigma_2 - \sigma_3|, |\sigma_3 - \sigma_1|), \tag{19}$$

where $\sigma_1, \sigma_2, \sigma_3$ are the principle stresses.

We calculate the deformations corresponding to $\tau_{\max}$:

$$\varepsilon_{\max} = \frac{(1+\nu)}{E}\tau_{\max}, \tag{20}$$

where ν is Poisson's ratio, E is Young's modulus.

3. Numerical results

Solving the integral (11) for an arbitrary smooth surface in an analytical form is difficult. Therefore, in the course of numerical calculations, the Clenshaw-Curtis quadrature method [25] was used.

3.1. Computational experiment No. 1

The fault surface was located at a depth of $C = 5000$ m, its linear dimensions were $L = 4000$ m, $W = 3000$ m, the displacement value Δu_1 was assumed to be constant and equal to 0.8 m. A grid of size 6×5 was set on the fault surface. The random variable in the grid nodes was normally distributed with the parameters $\mu = 0$ m, $\sigma = 350$ m. The isolines of the stochastic fault surface are shown in Figure 4.

Preprints (www.preprints.org) | NOT PEER-REVIEWED | Posted: 11 August 2023 doi:10.20944/preprints202308.0919.v1

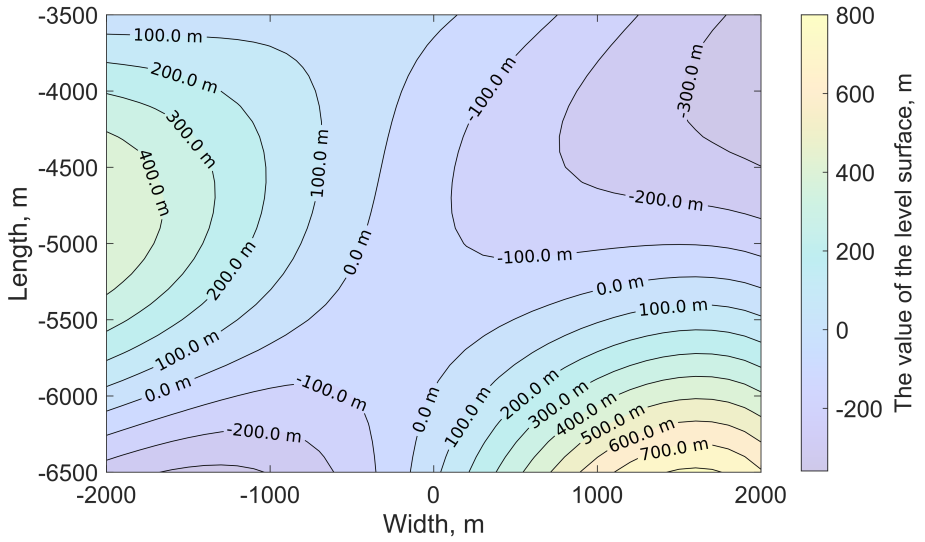

Figure 4. Fault surface level lines for computational experiment No. 1.

Figure 5 shows the relative deformations $\varepsilon_{\max}$ on the surface $x_3 = 0$, which are formed under the action of displacement along the stochastic surface. Figure 6 shows the relative deformations, which are formed under the action of displacement along the rectangular part of the plane.

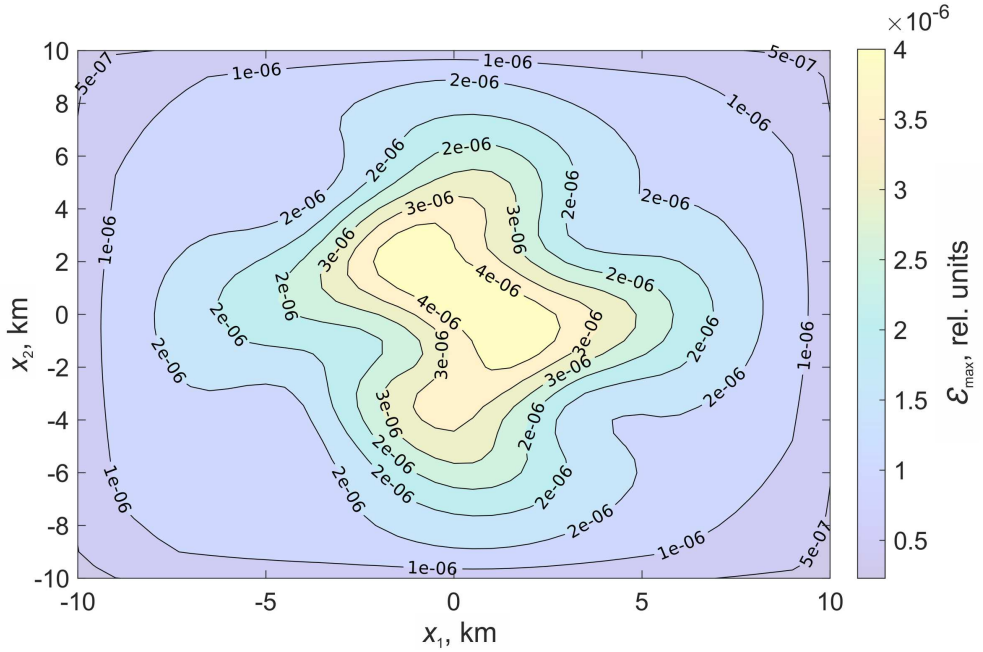

Figure 5. Relative deformations $\varepsilon_{\max}$ on the surface $x_3 = 0$ formed under the action of displacement on a stochastic surface.

Preprints (www.preprints.org) | NOT PEER-REVIEWED | Posted: 11 August 2023 doi:10.20944/preprints202308.0919.v1

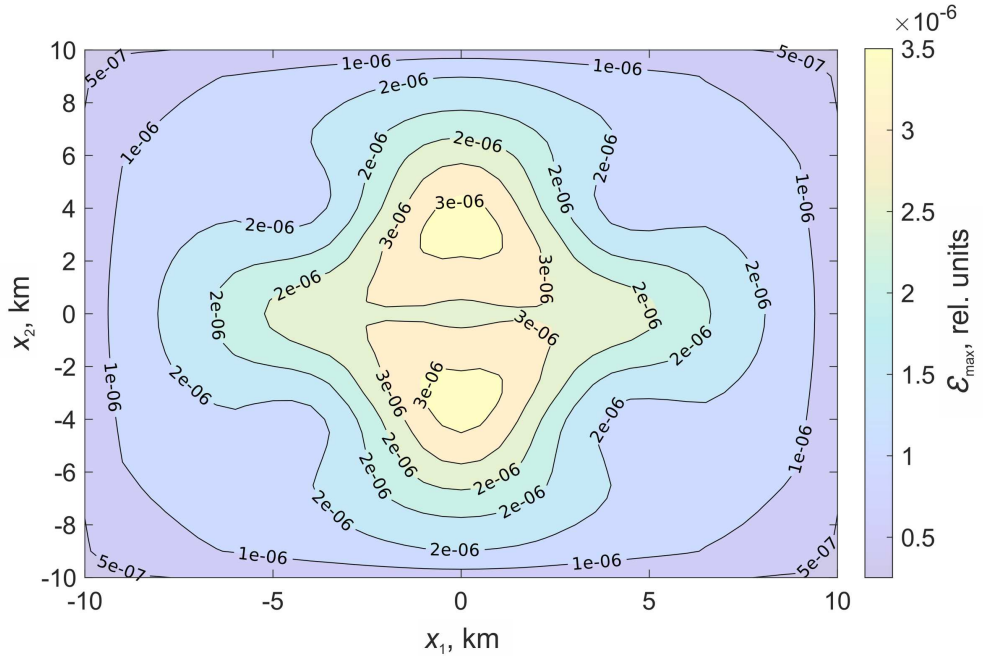

Figure 6. Relative deformations $\varepsilon_{\max}$ on the surface $x_3 = 0$ formed under the action of displacement along a flat surface bounded by a rectangular region.

In the case of a stochastic surface, the regions of relative deformations acquire a pronounced asymmetry. There is an increase in the deformation level in the center.

In addition, there are pronounced changes in the derivatives variations of the displacement field with a change in depth. For example, Figure 7 shows variations at depths up to 20 km ($x_1 = -2000$ m, $x_2 = 100$ m, x_3 varies from 0 to - 20000 m).

Preprints (www.preprints.org) | NOT PEER-REVIEWED | Posted: 11 August 2023 doi:10.20944/preprints202308.0919.v1

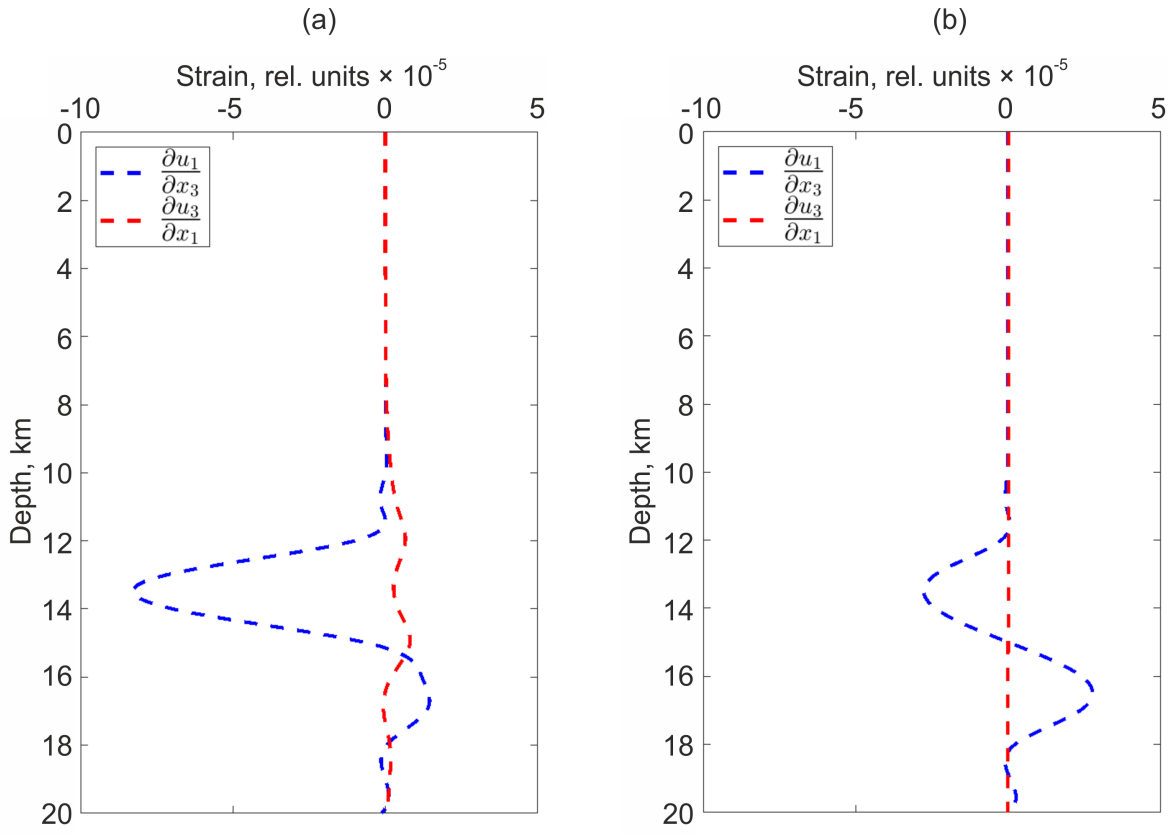

Figure 7. Depth dependency of $\partial u_1/\partial x_3$ and $\partial u_3/\partial x_1$ in the case of movement along the stochastic surface **(a)** and along the rectangular part of the plane **(b)**.

3.2. Computational experiment No. 2

The fault surface was at a depth of $C = 5000$ m, its linear dimensions were $L = 6000$ m, $W = 3000$ m, the displacement Δu_1 was assumed to be constant and equal to 1.5 m. A grid of size 7×5 was set on the fault surface. The random variable in the grid nodes is normally distributed with the parameters $\mu = 0$ m, $\sigma = 300$ m. The isolines of the stochastic discontinuity surface are shown in Figure 4.

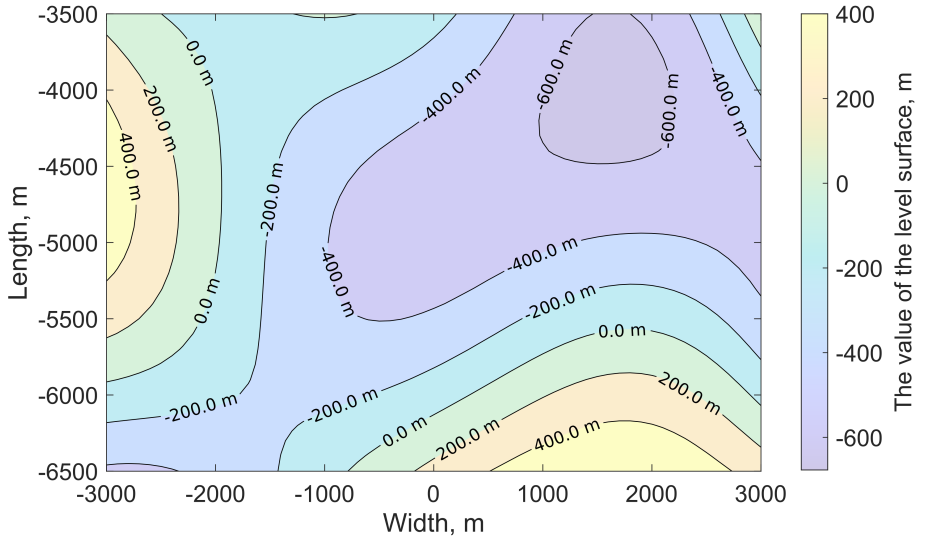

Figure 8. Fault surface level lines for computational experiment No. 2.

Preprints (www.preprints.org) | NOT PEER-REVIEWED | Posted: 11 August 2023 doi:10.20944/preprints202308.0919.v1

Figure 9 shows the relative deformations $\varepsilon_{\max}$ on the surface $x_3 = 0$, which are formed under the action of displacement along the stochastic surface. Figure 10 shows the relative deformations, which are formed under the action of displacement along the rectangular part of the plane.

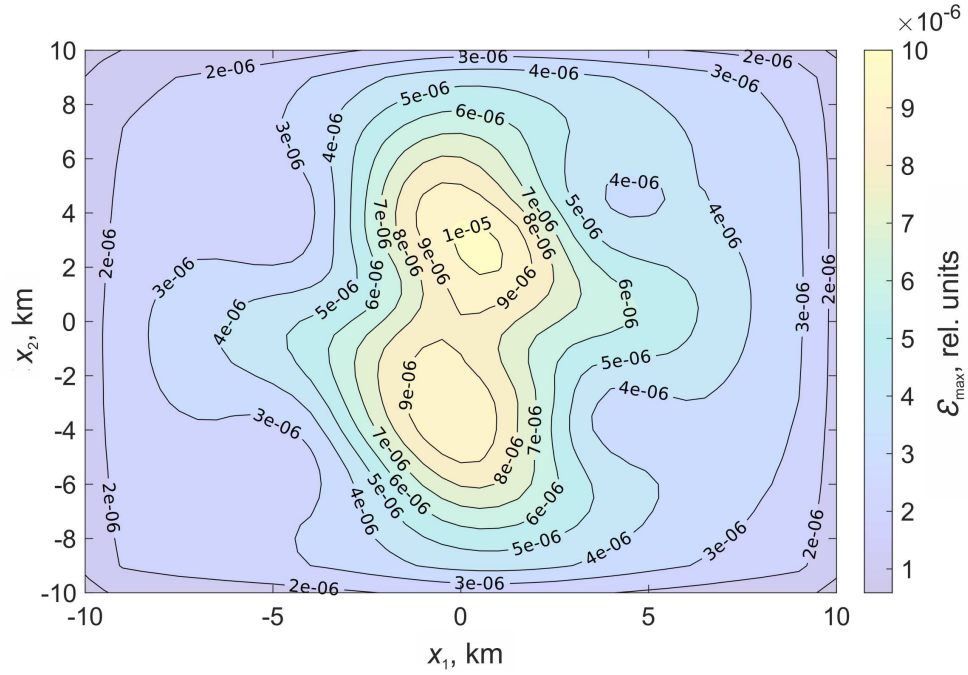

Figure 9. Relative deformations $\varepsilon_{\max}$ on the surface $x_3 = 0$ formed under the action of displacement on a stochastic surface.

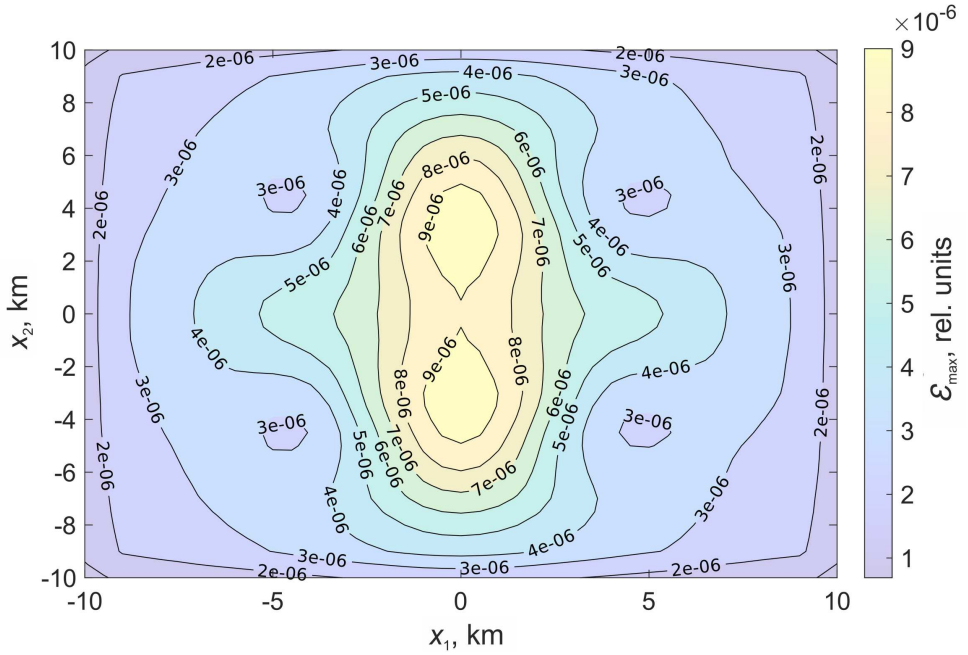

Figure 10. Relative deformations $\varepsilon_{\max}$ on the surface $x_3 = 0$ formed under the action of displacement along a flat surface bounded by a rectangular region.

As in the previous experiment, in the case of a stochastic surface, the regions of relative deformations acquire a pronounced asymmetry. There is a significant decrease in the deformation level in the area $-8 < x_1 < -5, -8 < x_2 < 8$. There are also differences in the rate of change

Preprints (www.preprints.org) | NOT PEER-REVIEWED | Posted: 11 August 2023 doi:10.20944/preprints202308.0919.v1

of the displacement field vector components in different directions. Figure 11 shows variations of displacement field derivatives, coordinates are similar to the previous experiment.

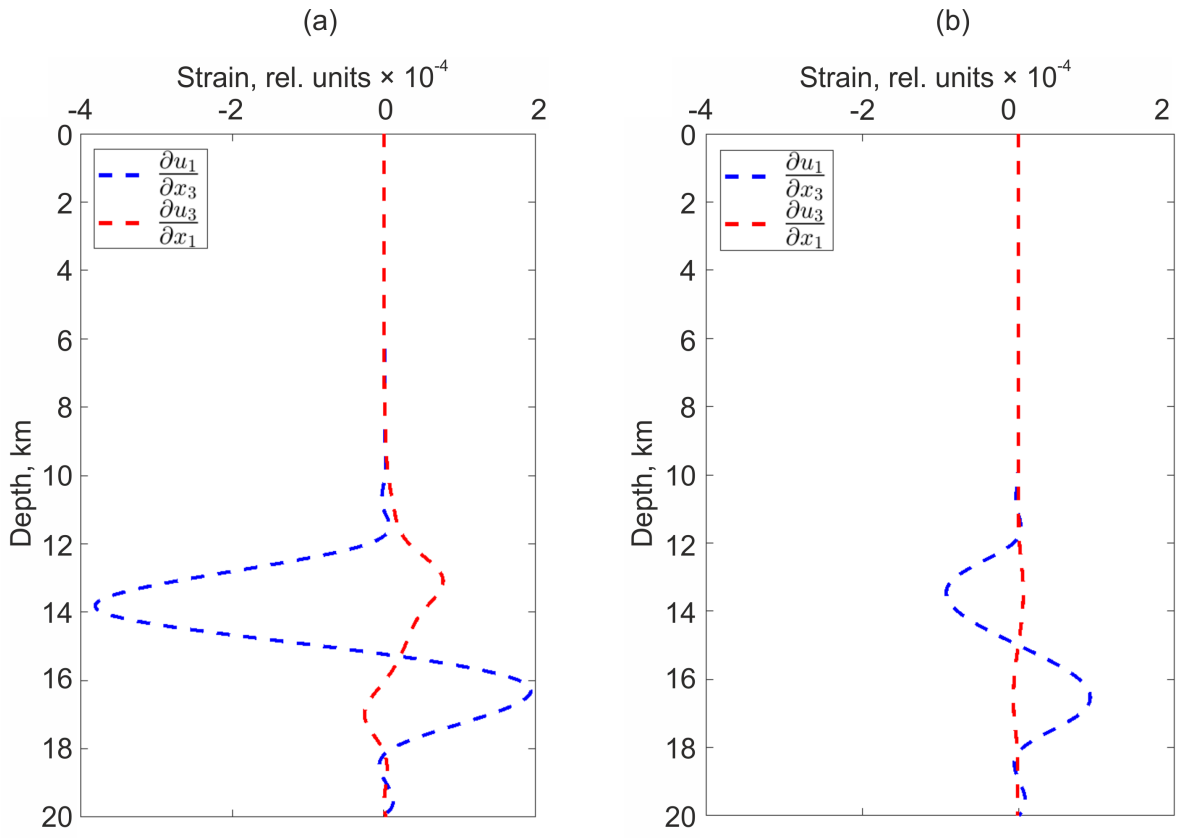

Figure 11. Depth dependency of $\partial u_1/\partial x_3$ and $\partial u_3/\partial x_1$ in the case of movement along the stochastic surface **(a)** and along the rectangular part of the plane **(b)**.

As an example, we consider the distribution of relative deformation areas (Figure 12) caused by a 2 m displacement along a 6x3 km fault surface located at a depth of 15 km. Such dimensions correspond to an earthquake with a moment magnitude of approximately $M_w = 6$ on the Kanamori scale. The Figure 12 shows a fragment of the Kamchatka Peninsula. This is one of the most seismically active regions of the planet. Most Kamchatka earthquakes occur at a distance of 30–150 km from the eastern coast of the peninsula, in the subduction zone adjacent to the Kuril-Kamchatka Trench. Let us assume that the epicenter of this hypothetical earthquake was located near the peninsula in the subduction zone (the epicenter coordinates are 52.85°N, 158.75°E).

It can be seen from the Figure 12b that in the case of displacement along a stochastic fault surface, deformations increase in the coastal zone. Therefore, their influence there will be higher. Such asymmetry of deformation regions can help explain why signals propagating from the earthquake source do not always reach the zones controlled by geophysical sensors.

Preprints (www.preprints.org) | NOT PEER-REVIEWED | Posted: 11 August 2023 doi:10.20944/preprints202308.0919.v1

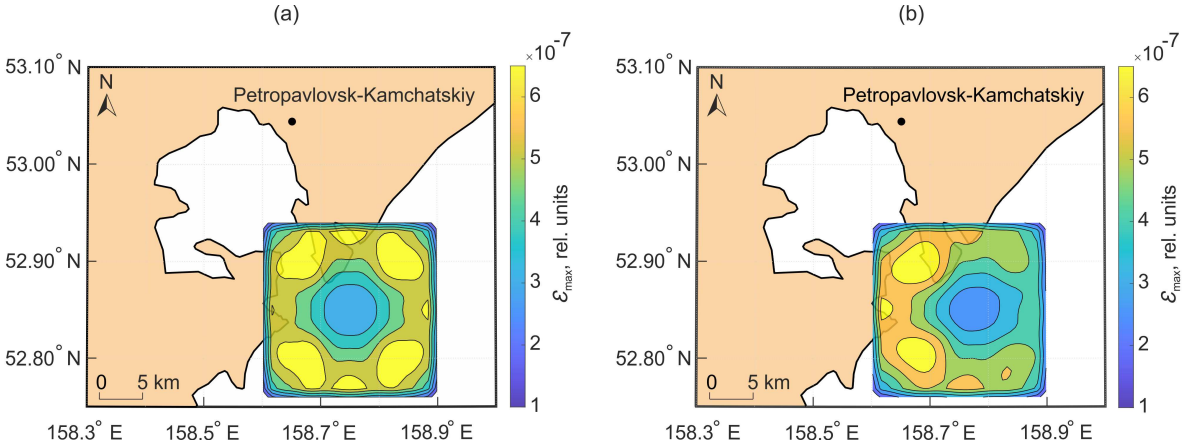

Figure 12. Relative deformations $\varepsilon_{\max}$ on the Earth's surface caused by a hypothetical earthquake with the moment magnitude $M_w = 6$. Deformations formed under the action of displacement along a flat surface bounded by a rectangular region **(a)** and along a stochastic surface **(b)**.

4. Conclusion

In this paper, we propose a model of an earthquake source in the form of a strike-slip displacement along a stochastic surface. To do this, a random component is introduced into the classical model, according to which the fault surface is represented as a flat rectangular area. It determines the random deformation of this area. The displacement vector is assumed to be constant. In the case of a stochastic fault surface, the regions of relative deformations acquire a pronounced asymmetry. Thus, adding a stochastic component will help indirectly take into account the heterogeneity of rocks when modeling deformations caused by earthquakes.

In the perspective of further research, we will consider a way to add a stochastic component to the geometry of the discontinuity plane. The presence of common statistical characteristics of the geometry of the surfaces of all earthquake sources seems unlikely. However, the presence of characteristics that directly or indirectly affect the shape of the fault surface is quite possible. In addition, the model can be complicated by adding a random displacement vector.

Author Contributions: Conceptualization, M.G.; methodology, M.G.; software, A.S. and M.G.; validation, R.P.; formal analysis, R.P.; investigation, M.G.; resources, M.G. and A.S.; data curation, A.S. and M.G.; writing—original draft preparation, M.G. and A.S.; writing—review and editing, R.P.; visualization, A.S. and M.G.; supervision, R.P.; project administration, M.G.; funding acquisition, R.P. All authors have read and agreed to the published version of the manuscript.

Funding: The research was carried within the framework of the State task on topic (2021–2023) "Physical processes in the system of near space and geospheres under solar and litospheric impact", registration number AAAA-A21-121011290003-0.

Conflicts of Interest: The authors declare no conflict of interest.

References

1. Sholz, C. *The mechanics of earthquakes and faulting*, 3rd ed.; Cambridge University Press: Cambridge, UK, 2019.
2. Steketee J. On Volterra's dislocations in a semi-infinity elastic medium. *Can. J. Phys.* **1958**, *36*, 192-205.
3. Kundu, P.; Sarkar, S.; Mondal, D. Creeping effect across a buried, inclined, finite strike-slip fault in an elastic-layer overlying an elastic half-space. *GEM - Int. J. Geomath.* **2021**, 12, 1–33.
4. Liu, T.; Fu, G.; She, Y.; Zhao, C. Co-seismic internal deformations in a spherical layered earth model. *Geophys. J. Int.* **2020**, *221*, 1515–1531.
5. Mondal D.; Debnath P. An application of fractional calculus to geophysics: effect of a strike-slip fault on displacement, stresses and strains in a fractional order Maxwell type visco-elastic half space. *Int. J. Appl. Math.* **2021**, *34*, 873–888.
6. Press, F. Displacements, strains, and tilts at teleseismic distances. *J. Geophys. Res.* **1965**, *70*, 2395–2412.

7. Saltykov, V.A.; Kugaenko, Y.A. Development of near-surface dilatancy zones as a possible cause for seismic emission anomalies before strong earthquakes. *Russ. J. Pac. Geol.* **2012**, *6*, 86–95.
8. Okada, Y. Internal deformation due to shear and tensile faults in a half-space. *Bull. Seismol. Soc. Am.* **1992**, *82*, 1018–1040.
9. Gusev A. Statistics of the values of the normalized movement at the points of the fault-the focus of the earthquake. *Phys. Earth* **2011**, *3*, 24–33. (In Russian).
10. Lekshmy, P.; Raghukanth, S. Stochastic earthquake source model for ground motion simulation. *Earthq. Eng. Eng. Vib.* **2019**, *18*, 1–34.
11. Zhang, G.; Wang, Z.; Sang, W.; Zhou, B.; Wang, Z.; Yao, G.; Bi, J. Research on Dynamic Deformation Laws of Super High-Rise Buildings and Visualization Based on GB-RAR and LiDAR Technology. *Remote Sens.* **2023**, *15*, 3651.
12. Ding, Y.; Xu, Y.; Ding, S. A Stochastic Earthquake Ground Motion Database and Its Application in Seismic Analysis of an RC Frame-Shear Wall Structure. *Buildings* **2023**, *13*, 1637.
13. Small, D. T.; Melgar, D. Geodetic coupling models as constraints on stochastic earthquake ruptures: An example application to PTHA in Cascadia. *J. Geophys. Res. Solid Earth* **2021**, *126*, e2020JB021149.
14. Gusev, A. Doubly stochastic earthquake source model: "Omega-Square" spectrum and low high-frequency directivity revealed by numerical experiments. *Pure Appl. Geophys.* **2014**, *171*, 2581–2599.
15. Peng, W.; Huang, X.; Wang, Z. Focal Mechanism and Regional Fault Activity Analysis of 2022 Luding Strong Earthquake Constraint by InSAR and Its Inversion. *Remote Sens.* **2023**, *15*, 3753.
16. Zhao, J.-J.; Chen, Q.; Yang, Y.-H.; Xu, Q. Coseismic Faulting Model and Post-Seismic Surface Motion of the 2023 Turkey–Syria Earthquake Doublet Revealed by InSAR and GPS Measurements. *Remote Sens.* **2023**, *15*, 3327.
17. Yu, S.; Su, X. A Crustal Deformation Pattern on the Northeastern Margin of the Tibetan Plateau Derived from GPS Observations. *Remote Sens.* **2023**, *15*, 2905.
18. Aki, K.; Richards, P. *Quantitative Seismology*, 2nd ed.; University Science Books: Cambridge, UK, 2002.
19. Molotnikov, V.; Molotnikova, A. *Theory of Elasticity and Plasticity*; Springer International Publishing: Cham, Switzerland, 2021.
20. Mindlin, R. Force at a point in the interior of a Semi-Infinite solid. *J. Appl. Phys.* **1936**, *195*, 195–292.
21. Mindlin, R.; Cheng, D. Nuclei of Strain in the Semi-Infinite Solid. *J. Appl. Phys.* **1950**, *21*, 926–930.
22. Pan P.-Z.; Miao, S.; Wu Z.; Feng X.-T.; Shao C. Laboratory observation of spalling process induced by tangential stress concentration in hard rock tunnel. *Int. J. Geomech.* **2020**, *20*, 04020011.
23. Wang C.; Wang S. Modified Generalized Maximum Tangential Stress Criterion for Simulation of Crack Propagation and Its Application in Discontinuous Deformation Analysis. *Eng. Fract. Mech.* **2022**, *259*, 108159.
24. Xiao, P.; Li, D.; Zhu, Q. Strain Energy Release and Deep Rock Failure Due to Excavation in Pre-Stressed Rock. *Minerals* **2022**, *12*, 488.
25. Clenshaw, C.W.; Curtis, A.R. A method for numerical integration on an automatic computer. *Numer Math* **1960**, *2*, 197–205.